POLITECNICO DI TORINO
Repository ISTITUZIONALE

An N-of-1 longitudinal and multimodal physiological dataset from para-handcycling training and endurance competition

Original
An N-of-1 longitudinal and multimodal physiological dataset from para-handcycling training and endurance competition / Spinazzola, E., Prono, L.. - In: SCIENTIFIC DATA. - ISSN 2052-4463. - ELETTRONICO. - (2026). [10.1038/s41597-026-08691-1]

Availability:
This version is available at: 11583/3018330 since: 2026-11-23T13:41:51Z

Publisher:
Springer

Published
DOI:10.1038/s41597-026-08691-1

Terms of use:

This article is made available under terms and conditions as specified in the corresponding bibliographic description in the repository

Publisher copyright

(Article begins on next page)

29 November 2026

scientific data

Article in Press

Check for updates

OPEN

DATA DESCRIPTOR

An N-of-1 longitudinal and multimodal physiological dataset from para-handcycling training and endurance competition

Elisabetta Spinazzola ✉ & Luciano Prono

Publicly available physiological datasets from individuals with Spinal Cord Injury (SCI) remain limited, particularly for longitudinal monitoring during rehabilitation and endurance sports activities. This work presents a longitudinal multimodal dataset of 42 recordings, each lasting between 1 and 9 hours, collected from one participant with paraplegia over seven months of para-handcycling training and endurance competition across Saudi Arabia. Physiological and environmental measurements were continuously acquired using a wearable monitoring device. Recordings included synchronized electrocardiographic, respiratory, acceleration, skin-temperature, environmental-temperature and oxygen-saturation data streams. Alongside the device-processed signals, the dataset provides processed recordings and derived physiological variables generated through standardized signal processing procedures to support plausibility checks and reuse. This N-of-1 longitudinal dataset is intended to support method development, signal-processing benchmarking, and hypothesis generation for personalized, participant-specific monitoring in SCI-related endurance exercise.

Background and Summary

Up to 20000 patients annually suffer a spinal cord injury (SCI) and about 20% die before hospital admission[1]. SCI refers to damage to the spinal cord that temporarily or permanently alters its function[2], often leading to paraplegia when lesions affect thoracic, lumbar, or sacral segments, impairing motor and sensory functions of the lower limbs and strongly impacting patients' physical health and quality of life[3]. Rehabilitation is therefore essential to maximize residual functional abilities and patient autonomy. However, outcomes depend on several factors, including lesion characteristics, physiological condition, comorbidities, and therapies, making patient-specific and adaptive rehabilitation protocols necessary.

Emerging technologies such as telehealth monitoring, clinical decision support systems, and mobile biosignal analyzers require large publicly accessible datasets[4–6]. In rehabilitation medicine, particularly for SCI, such datasets remain limited, especially regarding biosignal recordings collected in realistic physiological or functional conditions. Several clinical studies have investigated physiological parameters in SCI, such as Heart Rate (HR), peripheral oxygen saturation (SpO_2), Skin/Body and Environmental Temperature (T_{skin} and T_{env}) and Heart Rate Variability (HRV) power spectrum for fatigue analysis[7–12].

Moreover, paraplegic patients performing physical exercise have increasingly been recruited in advanced experimental protocols, particularly focusing on handcycling endurance[13–20]. For example, long-distance races have been studied, such as a 540km handcycling race by a single SCI participant[21]. Table 1 summarizes these studies, providing a brief overview of the state of the art, the existing gaps and the advances offered by our dataset.

Even though several studies have investigated SCI patients' physiological responses to exercise, publicly available longitudinal datasets containing multimodal recordings remain limited.

This scarcity restricts the development and validation of computational tools and may lead to therapeutic assumptions not fully supported by empirical evidence. In particular, physiological data collected from paraplegic individuals during daily activities or physical stress are gaining attention for improving rehabilitation strategies and patient independence[23–26].

Department of Electronic and Telecommunication, Politecnico di Torino, 10129, Torino, Italy. ✉e-mail: elisabetta.spinazzola@polito.it

Author	Subjects	Focus of the Study	Type of Exercise	Biosignals	Gap	Advancement of this dataset
Stephenson[14]	58 experimental case studies	Aerobic capacity and physiological determinants in handcyclists	Hand-bike riding	Distance, Speed, Time, Load, VO_2, HR, Aerobic power, Respiratory exchange ratio, Blood lactate	Limited open physiological datasets for reproducible research	Public release of a multimodal biosignal dataset for SCI endurance exercise
Fischer[13]	5 tetraplegic athletes; 12 paraplegic athletes	Bioenergetic and biomechanical parameters in ecological conditions	Race hand-bike	Speed, Power, Resistance	Focus on performance metrics rather than continuous physiological monitoring	Continuous wearable biosignal monitoring including ECG, respiration and SpO_2
Abel[21,22]	1 SCI participant	Physiological response during a long-distance 540km hand-bike race	Race hand-bike	Time, Workload, HR, Speed, Distance, Blood analysis	Limited physiological signal diversity and short monitoring duration	Extended monitoring across months of training and a 3000km endurance race
Chou[20]	–	Cardiovascular response to body temperature variations	–	T_{skin}, T_{env}, HR	Controlled laboratory conditions with limited ecological exercise data	Real-world physiological monitoring under extreme environmental conditions
Hertig[18]	15 athletes with tetraplegia or paraplegia	Thermoregulatory and sweat responses in SCI individuals	Various exercises	T_{skin}, HR	Lack of integrated multi-biosignal and environment datasets during prolonged endurance activity	Multimodal dataset combining cardiovascular, respiratory, thermal signals and environmental conditions
Yamasaki[17]	12 SCI subjects (T3-L2); 7 able-bodied	Body temperature regulation in paraplegics	Arm cranking exercise	T_{skin}, T_{env}	Short-duration experiments in controlled environments	Long-duration ecological monitoring during endurance training and racing
Kenny[19]	–	Review on post-exercise thermoregulation in SCI	–	T_{skin}	Lack of large-scale physiological datasets for validating thermoregulation models	Dataset enabling multimodal modeling and machine learning approaches

Table 1. Overview of related studies on physiological monitoring in handcycling and SCI exercise.

In this context, we present an N-of-1 longitudinal and multimodal dataset collected from an individual affected by stable lumbosacral partial SCI-induced paraplegia who performed seven months of structured hand-bike training including a 3000km endurance race across Saudi Arabia. The experiment involved continuous biosignal acquisition through a wearable device (Healer R3 by L.I.F.E. Italia S.r.l.), recording electrocardiographic (ECG), respiration, blood oxygen saturation, acceleration, axillary skin and environment temperature signals. The dataset, publicly released on Zenodo (DOI: 10.5281/zenodo.23168228)[27], consists of 42 recordings collected over seven months (July 2023 – January 2024), each lasting between 1 and 9 hours.

The dataset preparation pipeline is shown in Fig. 1, guided by the intention of following the Findability, Accessibility, Interoperability and Reusability (FAIR) principles[28], necessary to fully exploit the capacity of computational systems to operate on data with no or minimal human intervention.

The dataset was analyzed to assess the physiological and clinical evolution of the subject through the description of the experimental protocol and is accompanied by contextual information to facilitate correct interpretation and reuse. As a single-participant longitudinal dataset, this resource does not capture the physiological heterogeneity of the SCI population, including variability in lesion level and completeness, autonomic dysfunction, sex, age, training status, comorbidities, medication use, thermoregulatory impairment, and rehabilitation stage. The dataset is therefore best suited for hypothesis generation, N-of-1 modeling approaches, and methodological/signal-processing development, rather than for deriving generalizable clinical conclusions.

Methods

Ethics statement. The study was conducted within a broader research protocol, which involved the acquisition of physiological data from the same participant using different wearable sensing systems. As the experimental activities were primarily conducted in Saudi Arabia, including both indoor sessions at the King Abdullah University of Science and Technology (KAUST) campus and outdoor activities under extreme environmental conditions, the protocol was submitted to and approved by KAUST Institutional Biosafety and Bioethics Committee (IBEC) at KAUST, as the lead investigation site, under IBEC Number: 23IBEC092, approved on December 18, 2023. The approval covers both the prospective and the retrospective data collection.

However, the specific experimental procedures and dataset presented in this manuscript were independently acquired, curated, and analyzed by the authors of the present study.

Written informed consent was obtained from the subject prior to participation in the study for data collection, publication and sharing of anonymized data. The study was conducted in accordance with the Declaration of Helsinki.

Politecnico di Torino was neither the recruiting institution nor the institution responsible for the ethical oversight of the experimental data collection.

Because of this, Politecnico di Torino declared that no additional ethical approval or permission for the activities of this study was required.

Participant. After considering all the procedures and possible risks associated with the investigation, the subject decided to enroll in the proposed experiment, aware of being the only participant. He is a 42-year-old male

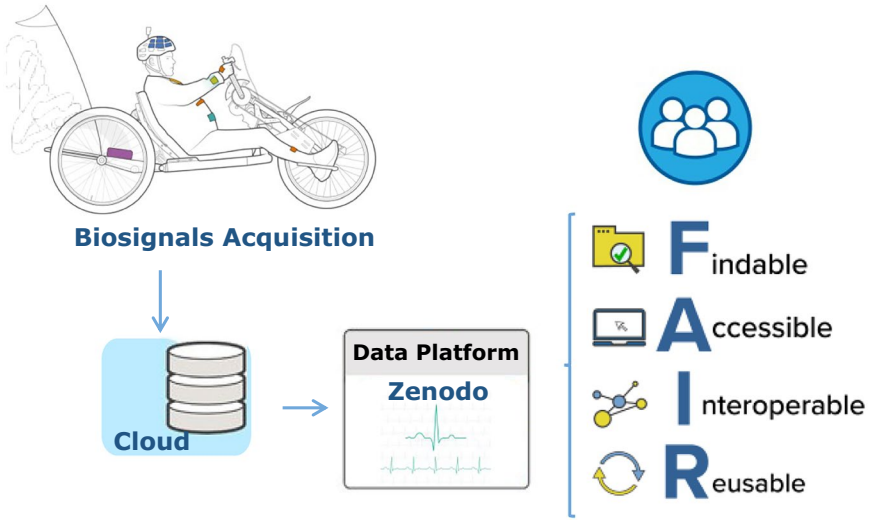

Fig. 1 Biosignals dataset preparation pipeline: from the data acquisition to the dataset publication, under the FAIR principles.

weighing 79kg with lumbosacral partial, stable SCI damage. AIS grade, neurological level and time since injury are withheld deliberately for anonymization. The participant was not an active athlete before his SCI occurred. Instead, after the rehabilitation, he started performing outdoor racing, improving his endurance. All training sessions were planned and supervised by the clinical team of the Villa Beretta Rehabilitation Research Innovation Institute (VBRRII), which followed his rehabilitation program. Due to the N-of-1 nature of the dataset, the participant's physiological responses reported throughout this work should be interpreted as individual-specific case of study.

Experimental protocol and instrumentation. This study lasted seven months: a training period (July-December 2023) culminating in the first hand-bike ride across Saudi Arabia (December 2023-January 2024). The subject undertook a 30-day journey from east to west, cycling over 3000 km during the second half of December 2023 until the first half of January 2024. He began his journey in Dammam and concluded at KAUST campus, passing through major cities and regions including Riyadh, Buraydah (Qassim), Hail, AlUla, Red Sea Global, Al-Madinah, Makkah, Jeddah, and finally KAUST.

Hand-bike. Handcycling, as the target rehabilitation activity, was selected as a representative functional modality to perform controlled upper-limb exercise in individuals with SCI[15]. This type of exercise can be performed outdoors and is suitable for early-stage rehabilitation, thereby supporting the development of active and healthy lifestyle habits[14].

For the study, the participant employed the CrossWind XE hand-bike by Maddiline Cycle Snc (https://www.maddilinecycle.com/en) and the HP Scorpion FS 26 Enduro trike (https://www.hpvelotechnik.com/en/recumbent-trikes-bikes/scorpion-adults-recumbent-trikes/scorpion-fs-26-enduro-offroad-trike/for more information). More specifically, these are tadpole trikes, which are part of a much larger class of human-powered vehicles called recumbents.

In addition, the participant employed functional electrical stimulation (FES). FES stimulates the physiological movements of the muscle groups involved, enabling limb movement even with reduced or absent neural connectivity. Specifically, he used the portable VIK8 solution with the Adaptive Functional Electrical Stimulation Kinesitherapy technology (AFESK), developed by VIKTOR S.r.l. This device can reproduce, support and maximize any complex cyclical movement, such as cycling with a bicycle, hand-bike, or trike. Data were sent daily to VBRRII, in order to closely monitor the patient's conditions.

Healer Wearable Device. We employed the *Healer* wearable medical device (Class IIa) by L.I.F.E. Italia S.r.l[29] to collect the training and race biomedical data. *Healer* is made of synthetic, elastic and breathable technical fabric that integrates a series of sensors for detecting physiological parameters and signals. It is intended for multiparametric monitoring applications and examinations. The device includes a data logger and cloud platform (Healer Cloud) for data storage and processing. In the study, the subject used the Healer R3, whose sensor-equipped garment records a set of different physiological signals, as shown in Fig. 2.

The recorded signals are:

- *ECG signals*: they are acquired with 10 dry electrodes to obtain the standard 12-lead ECG signals at a sampling frequency of 500Hz. Configuration of the electrodes follows the Einthoven triangle[30]. Fig. 3 shows that four electrodes are placed on the extremities of the right arm (RA), left arm (LA), right leg (RL), left leg (LL). Moreover, six precordial electrodes (V1-V6) are placed on the chest. The RL electrode is used as a ground or reference electrode to help complete the circuit and reduce electrical noise. The 12 leads are composed of 6

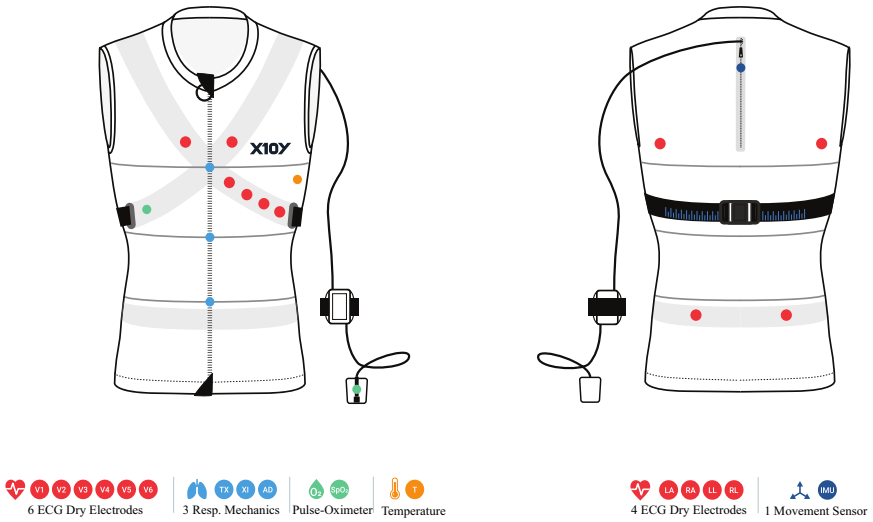

Fig. 2 The *Healer R3* sensorized device employed to record the physiological parameters. Adapted from the device manual[29], available in the Zenodo repository[27].

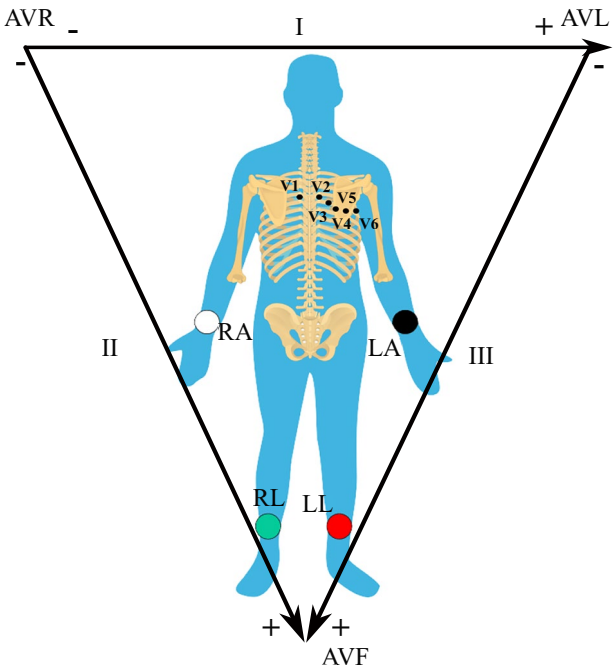

Fig. 3 Einthoven triangle and leads.

precordial leads (V1-V6), 3 standard limb leads (I, II, III) and 3 augmented limb leads (AVR, AVL, AVF). The limb leads and augmented limb leads are calculated from the voltages between different pairs of the 4 limb electrodes. The limb leads are monopolar leads, referring to the fact that one electrode is the active recording electrode, and the other electrodes serve as references. With the same 4 limb electrodes, it is possible to evaluate 3 bipolar leads: the lead I (potential difference between the left arm (LA) and the right arm (RA)), the lead II (potential difference between the left leg (LL) and the right arm (RA)) and the lead III (potential difference between the left leg (LL) and the left arm (LA)). The augmented limb leads correspond to Augmented Voltage Right arm (AVR), Augmented Voltage Left arm (AVL) and Augmented Voltage Foot (AVF) leads, respectively. These come from a special type of electrode configuration called augmented unipolar leads and derive from the same four limb electrodes using a special augmentation technique. Finally, the precordial leads are positioned in 6 chest electrodes, referred to as V1, V2, V3, V4, V5 and V6. They are used to better recognize alterations of the anterior and posterior walls of the left ventricle. As shown in Fig. 2, the electrodes' placement differs from the position described in Fig. 3. The device uses the Modified Limb Lead Placements

Analysis	Description
HR [beat/min]	Number of detected R peaks in one minute of ECG signal
RR [breaths/min]	Number of detected peaks in one minute of respiration signal
T_{skin} and T_{env}[°C]	Axillary skin and environment temperature after processing
SpO_2 levels	Classification of SpO_2 into optimal, good and poor ranges

Table 2. Data Analysis Steps.

Configuration, a common modification in which the upper limb electrodes are placed on the shoulders or forearms and the left leg electrodes are placed on the abdomen, usually at the lower quadrant.

- *Respiratory signals*: clinicians record breathing patterns to identify dysfunctional breathing. Respiratory signals are recorded with three strain-gauge circumferential sensors placed at the thoracic, xiphoid and abdominal levels, sampled at 50Hz. Respiration belt sensors placed around the thorax (chest) and abdomen are used to measure increases and decreases in the expansion of the chest and abdomen associated with breathing[31]. The units of strain gauge lengthening/shortening are relative units. The voltage output of a strain gauge is proportional to the increase in distance between the attachment points of the stretchable rubber tube. The signal is amplified and displayed as the respiratory signal in relative units of 0 to 100, called Relative Units of Stretch (RUS) voltages[32].
- *Axillary skin and environmental temperature* (T_{skin}*and*T_{env}) *signals*: they are measured by means of two contact sensors under the right armpit at 1Hz sampling frequency. The most common methods for measuring body temperature include oral, axillary (underarm), tympanic (ear) and rectal thermometers, each with different accuracy levels. In this case, a thermistor-type contact thermometer provided real-time and non-invasive temperature tracking. This contact-skin sensor measures what is more properly an axillary/skin temperature rather than "body temperature". Therefore, we refer to these data as T_{skin} for simplicity.
- *Oxygen saturation*SpO_2*signals*: they are recorded with an optical module under the left armpit sampling at 1Hz. The SpO_2 is a non-invasive measurement, which evaluates the percentage of hemoglobin binding sites in the bloodstream occupied by oxygen using pulse oximetry. This technique relies on the differential absorption of Red and Infrared (IR) light by oxyhemoglobin (O_2Hb) and deoxyhemoglobin (HHb)[33].
- *Mechanical acceleration*: it is measured by means of a 9-channels Inertial Measurement Unit sensor (IMU) placed on the subject's back, sampling at 100Hz.

All the sensors are controlled by dedicated electronics, which are enclosed within a plastic shell (the wearable device connector) located in the rear of the Healer device.

Data processing. In order to properly process and analyze the recorded data and extract physiological features, we first produced a clean version of the dataset, focusing on motion artifacts and denoising, which play a prominent role in ECG signals[34]. The clinically relevant aspects are described in the following subsections. Table 2 provides a concise summary.

Prior to the denoising and feature-extraction procedures described below, we visually inspected all recordings to confirm the absence of missing data segments and overt cardiac anomalies, and to verify timing synchronization and sampling-rate agreement carried out with the support of the clinical team of the Villa Beretta Rehabilitation Research Innovation Institute (VBRRII), who supervised the participant's physiological status throughout the study.

We state that no acquisition-level missing data were identified in the delivered dataset; residual invalid segments arise only from the quality-based exclusion criteria described in the following section for each modality (motion-artifact segments for ECG/respiration (smoothed with denoising technique), physiological-range flagging for temperature, device-native quality indices for SpO_2). These excluded segments were omitted from the corresponding minute-level variable rather than imputed, especially for temperature and SpO_2 data.

All pre-processing and feature-extraction steps were applied identically across all 42 recordings. In particular, the ECG analyses reported throughout the manuscript – R-peak detection, HR, Pulse-Respiration Quotient (PRQ) – were performed on the same designated channel (lead II) for every session, and the output signals '.h5' files follow the same channel structure irrespective of garment model, ensuring a uniform processing pipeline across the entire dataset.

ECG and Respiratory signals. ECG signal amplitude typically ranges from 0.4 to 5mV, with frequencies between 0.5Hz and 100Hz. ECG recordings are particularly susceptible to motion artifacts, which have been mitigated prior to analysis[34]. For this reason, we intentionally avoided the use of complex denoising approaches, since the absence of a gold-standard reference signal for both ECG and respiration signals prevents us from objectively validating the filtering performance. We adopted a simple filter-based method, which represents a widely accepted, robust, and reproducible solution in physiological signal processing[35,36]. Specifically, we processed the ECG using a second-order Butterworth band-pass Infinite Impulse Response (IIR) filter with a low cutoff frequency of 4 Hz and a high cutoff frequency of 20 Hz (4-20 Hz). We implemented the filter using forward-backward filtering (zero-phase filtering) to avoid a net phase shift and, consequently, a systematic temporal displacement of the R-peaks. This specific design choice allows the same filtered signal to be used safely for peak localization without biasing R-to-R interval timing.

We designed the filtering for robust QRS enhancement and R-peak localization under motion conditions, rather than for preservation of the complete ECG morphology. The choice of the 4 Hz lower cutoff was

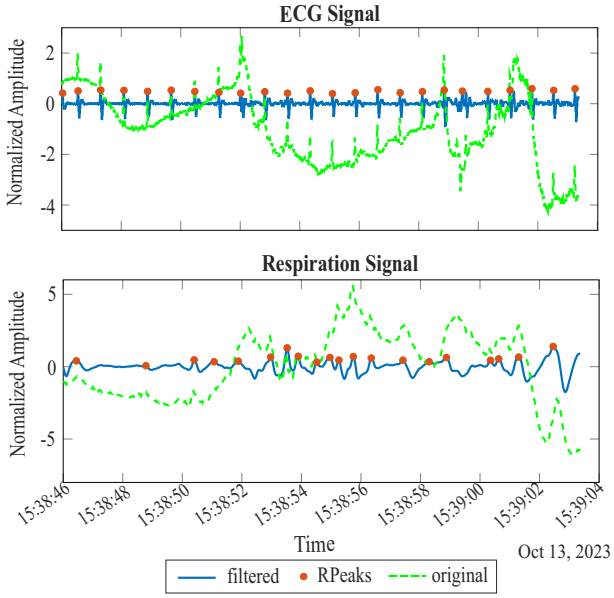

Fig. 4 ECG lead II and respiration signal processing, including denoising and peak extraction. The amplitude of the filtered signals was normalized with respect to the original one.

motivated by the characteristics of the experimental recordings. Since the ECG was acquired during movement, low-frequency components associated with baseline wander and motion-induced disturbances could substantially affect the plausibility of QRS localization. Increasing the lower cutoff to 4 Hz allowed these slow components to be attenuated while retaining the frequency content relevant to the relatively sharp QRS complexes. The upper cutoff of 20 Hz was selected to retain the principal QRS frequency content while attenuating higher-frequency noise, including muscle and instrumentation-related components.

The main physiological variable derived from ECG signals is HR. It was computed from the occurrence of successive R peaks[37]. In particular, the analyses on the ECG signals were performed on the lead `12`, from which we detect the peaks in the PQRST complexes. We applied an adaptive threshold that varies across ECG segments. The peak detections were implemented with the tools described in[38–40]. The clinical team checked the consistency of the obtained detections. In addition to the amplitude-based thresholding already described, R-peak detection was constrained by a minimum inter-peak distance criterion (corresponding to a physiological upper bound on HR), rejecting spurious peaks that would otherwise arise from residual high-frequency noise within the filtered signal. Once the PQRST complexes were detected, we derived the HR from the number of R peaks for each minute of recording.

Importantly, we used only the filtered ECG for R-peak detection. To assess the potential influence of filtering on R-peak localization, we additionally evaluated the detected R-peaks against the corresponding peaks identified in the original ECG. As Fig. 4 shows, we performed the comparison by matching R-peaks within a predefined temporal tolerance and visually evaluating the agreement in their temporal locations with respect to the original ECG, alongside the clinical team, who assessed the R-peak detection internal consistency. The evaluation did not reveal any R-peak distortion in time.

Similarly, one of the main aspects of the respiratory signals is the number of breaths per minute, called Respiration Rate (RR [breaths/min]). Over the last twenty years, many researchers have explored the possibility of deriving the RR by exploiting the influence of respiration on HR or ECG beat morphology, using respiratory sinus arrhythmia or respiratory peak amplitude waveforms[32,41–45]. We followed a similar procedure to estimate RR from the respiratory signals. In this case, the peak detection has been performed on the sum of the thoracic, xiphoid and abdominal signals. The RR was calculated as the number of the signal's peaks in one minute.

Figure 4 illustrates an example of the signal denoising and peak detection, both for the ECG `12` lead and the sum of the respiratory signals.

The derived HR and RR features form a minute-by-minute time series. Specifically, HR and RR were computed over consecutive, non-overlapping 60-second windows (30000 samples at the 500 Hz ECG sampling frequency). No resampling, interpolation, artifact-rejection thresholding or missing-data imputation was applied, other than the missing-data check and visual inspection described above. Artifacts and motion have been smoothed with the described filtering, while the one-sample-per-minute resolution was not obtained by resampling/decimating a higher-resolution derived signal, but by direct computation of each physiological variable within consecutive 60-second windows of the original signal.

Temperature and Oxygen saturation. Some temperature recordings (1 September, 10 September-1 October and 6 October-11 December) are affected by poor quality and corrupted acquisition, because of undetected device damage. For this reason, we performed a preliminary data processing to remove poor-quality or erroneous data, especially for temperature and SpO_2 fields. In this phase, we identified and removed data points that fall outside a predefined physiological range. Body temperature is a vital sign, reflecting the balance between heat production

Signal group	Description	Dataset entries	Mean ± Std
.ACCELEROMETER_3D	Acceleration in *x*, *y* and *z* directions.	.x [ms^{-2}] .y [ms^{-2}] .z [ms^{-2}] .t [s]	0.20 ± 1.47 8.52 ± 1.82 -2.35 ± 2.93
.ECG_LEAD_OFF_8_CH	Monopolar leads la, ll and ra (Fig. 3).	.la [mV] .ll [mV] .ra [mV] .v1-v6 [mV] .t [s]	4.34 ± 0.81 4.19 ± 0.77 4.04 ± 1.2 – –
.ELECTROCARDIOGRAM_8_CH	Precordial leads v1-v6 and bipolar derived limb leads I and II (Fig. 3).	.l1 [mV] .l2 [mV] .v1-v6 [mV] .t [s]	0.17 ± 9.15 4.17 ± 1.15 – –
.RESPIRATION_3_CH	Respiratory measurements acquired from abdominal, thoracic and xiphoid sensors.	.abd [RUS] .trx [RUS] .xif [RUS] .t [s]	2.38 ± 0.10 1.65 ± 0.082 1.61 ± 0.082 –
.SPO2	Pulse oximetry measurements including oxygen saturation, perfusion index, signal quality and status indicators.	.spo2_eng [%] .spo2_perfusion_eng [%] .spo2_quality_eng [%] .spo2_status_eng .t [s]	95.20 ± 2.49 94.49 ± 25.06 36.19 ± 37.92 10.99 ± 9.55 –
94.49 ± 25.06 36.19 ± 37.92 10.99 ± 9.55 –.TEMPERATURE	Dual temperature measurements used to derive T_{skin} and T_{env}.	.t1 [°C] .t2 [°C] .t [s]	36.88 ± 0.67 30.52 ± 5.41 –

Table 3. Structure of the HDF5 recordings (original signals) and descriptive statistics of the recorded signals (time and precordial leads have been omitted for simplicity).

and heat loss in the body. The standard T_{skin} hovers around 36°C, although more generally it ranges from 34 to 42°C, depending on factors such as the time of day, age, and activity levels. We used these values to detect when the device was damaged and removed non plausible values from the processed records. Then, we excluded the segments in which temperature had not yet stabilized, because the sensor had just come into contact with the subject's body.

For the SpO_2 data, the wearable device did not provide the raw optical pulse wave signal. However, it offers a quantitative assessment of the consistency of the extracted SpO_2, that we used to select the segments to be removed from the cleaned dataset (`spo2_quality_eng`, `spo2_status_eng`). We used the recorded SpO_2 quality data, described in Section Data Records, to clean SpO_2 signals.

Finally, since the SpO_2 levels are essential in assessing a person's oxygenation status, these were assessed for all the SpO_2 records. Healthy individuals typically have SpO_2 levels between 95% and 100%. Levels between 90% and 95% are still considered a sufficient SpO_2 status. Below 90%, the level shows a state of hypoxemia, a condition that requires medical attention. We considered this aspect for the analysis of training and race records.

Data Records

The dataset[27] comprises 42 records, of which 36 are related to the subject's training phase from July to the first half of December 2023, while the remaining 6 were recorded during the race period from the second half of December 2023 to January 2024. Each record corresponds to a different session (either during training or race). The dataset contains a total of 23 original device-processed biosignals, which are publicly available in the Zenodo repository v4.0[27] with DOI 10.5281/zenodo.23168228. To help users identify the appropriate level of the dataset for their intended reuse and distinguish from measured data, author-processed variables and exploratory analyses, the released data in the Zenodo repository[27] and accompanying documentation are organized into distinct files:

1. .h5 files: original device-processed signal recordings stored in Hierarchical Data Format 5 (HDF5) format, named by the acquisition date, described in Section Methods and as described below and in the Data Dictionary Table 4;
2. Variable.mat: processed physiological variables described in Section Methods and derived from inspected data, so excluded samples are not included;
3. PRQ.mat: results of the processed physiological variables described in the following Section Technical Validation;
4. MATLAB scripts supporting data visualization and signal pre-processing described in Section Methods (filtering, denoising, and peak-detection procedures applied to original signals). We also provide two Python scripts with the proof-of-concept examples of Section Data Overview.

File .h5: Original data. Each recording is stored as an HDF5 file and can be inspected in MATLAB using the `h5info` function. The root group contains file-level attributes, including the file version, a unique identifier, and the data source. Physiological signals are organized into separate HDF5 groups according to the sensor modality. Each modality contains one device-specific subgroup, identified by a hexadecimal code, and one time vector `t`. Signal values are stored either as native values `v` or engineering values `vEng`, depending on the channel. They contain data structured as reported in Table 3.

Specifically, as previously mentioned, a brief description of the recorded signals is provided to facilitate data use:

- The `.ELECTROCARDIOGRAM_8_CH` group contains the high-sampling-rate electrocardiographic recordings. It includes the limb leads `.l1` and `.l2` and the precordial leads `.v1` to `.v6`. These signals were recorded at 500Hz of sampling frequency. They measure the electrical activity of the heart over time, providing information about HR, rhythm, and potential abnormalities such as arrhythmias or ischemic events.
- The `.ECG_LEAD_OFF_8_CH` group contains lower-sampling-rate electrocardiographic monitoring channels and lead-off information. The available channels include `.la`, `.ll`, `.ra`, and `.v1` to `.v6`. Since these signals are intended only for well-being estimation, they were acquired at 1Hz.
- The `.RESPIRATION_3_CH` group contains respiratory measurements acquired from abdominal, thoracic, and xiphoid sensors. These channels are stored in the `.abd`, `.trx`, and `.xif` subgroups. These capture data related to breathing patterns, including rate, depth, and variability, which can help assess lung function and detect respiratory disorders. These signals have been recorded at 50Hz of sampling frequency.
- The `.TEMPERATURE` group contains two temperature channels, `t1` and `t2`, each stored in a separate device-specific subgroup. These channels were used to derive T_{skin} and T_{env} measurements, respectively. T_{skin}, in particular, monitors an axillary/skin temperature, which can indicate thermoregulatory responses, fever, inflammation, or metabolic activity. The two recordings refer to a dual temperature sensor. The T_{skin} is affected by the ambient temperature due to the design of the sensor. Therefore, an additional sensor has been added to measure the T_{env}, which in turn is affected by the T_{skin}. As a matter of fact, `t1` turns out to differ from `t2` by a maximum of 3.46°C. For this reason a signal quality assessment and correction were performed. These signals have been recorded at 1Hz of sampling frequency.
- The `.SPO2` group contains pulse oximetry measurements. SpO_2 represents the percentage of oxygen-saturated hemoglobin in the blood and provides information about the body's oxygenation status, making it a useful parameter for assessing respiratory efficiency. The oxygen saturation values are stored in `.spo2_eng`, while perfusion, signal quality, and status indicators are stored in `.spo2_perfusion_eng`, `.spo2_quality_eng`, and `.spo2_status_eng`, respectively. These signals have been recorded at 1Hz of sampling frequency.
- The `.ACCELEROMETER_3D` group contains three-axis acceleration data. The `.x`, `.y`, and `.z` subgroups include the acceleration signals along the corresponding spatial directions. These measure body motion and orientation along the three spatial directions, providing information about movement intensity, posture changes, vibration, and activity patterns during training and competition. The signals have been recorded at 100Hz of sampling frequency. The `.x`-axis corresponds to the transverse (horizontal) plane, the `.y`-axis to the longitudinal (vertical) plane, and the `.z`-axis to the sagittal plane. In this configuration, the `.y`-acceleration signal indicates the gravitational acceleration ($9.8ms^{-2}$) along with any jumps or undulations of the ground. The `.x`-acceleration revealed a mean approximately $0ms^{-2}$, indicating no acceleration in that direction (as expected), while the `.z`-acceleration corresponds to the direction of motion. We can also infer the sensor orientation from the acceleration data: as an example, we observe a negative contribution in the `.z`-acceleration due to the angle caused by the inclination of the seated position of the hand-bike.
- The time vector `.t` is also associated to each dataset field. The duration of the records varies between sessions, ranging from 1h to 9h. The Healer device timestamps the acquired data using a specific Greenwich Mean Time (GMT), enabling the further assessment of T_{skin} in relation to environmental conditions during training or race sessions. The time was set to the original GMT, which corresponds to GMT+3 hours for Saudi Arabia. For the proposed processing, 3 hours were added to the original timestamp.

Finally, the Table 3 reports the mean and standard deviation of the recorded signals after the pre-processing procedures described above.

Original signals data dictionary. The original signals provided by the device are stored in the *.h5* files, as device-processed output. In this dataset, original signals refer to signals provided by the device/software after device-level processing, but before any author-applied processing or feature extraction.

To further support dataset reuse and reproducibility, we provide a complete signal-level data dictionary in Table 4, consolidating the channel name, unit, nominal sampling frequency, anatomical sensor placement, device model, valid physiological/technical range, timestamp format, and processing status (original, filtered, derived, or inspected) for every signal group described in this manuscript. This data dictionary is also provided in the Zenodo repository[27], to facilitate programmatic access.

Sessions-level metadata. Beyond signal-level documentation, dataset reuse for physiological modeling benefits from session-level contextual metadata. Table 5 summarizes, for each of the metadata fields commonly relevant to this kind of dataset (recording date, training/race phase, session duration, known acquisition issues, sensor model, route information, weather conditions, time of day, equipment used, FES use, and rest periods), whether this information is available for the 42 recordings comprising this dataset. While several fields are readily available or derivable from the original device-processed data itself, others – notably GPS-derived route, distance, structured rest-period logs, and FES signals – were not part of the acquisition or record-keeping configuration adopted during this study and could not be reliably reconstructed retrospectively. We report this transparently so that prospective users can assess the suitability of the dataset for their intended reuse case.

Variable.mat. The file *Variable.mat* contains a MATLAB table named `DataTable`, where each row corresponds to a one-minute observation obtained from the multimodal physiological recordings. All variables are synchronized and expressed in common temporal resolution of one sample per minute, facilitating longitudinal analyses and multimodal data fusion.

Original Signal (device processed)	Channel & Unit	Freq. (Hz)	Body pos.	Healer model	Valid range	Author processed vars	Processing pipeline
ECG l1, l2	`.ELECTROCARDIOGRAM_8_CH` [mV]	500	Chest	R3	0.4–5	HR, PRQ	Denoising + Peak detection + Quality check
ECG la, ll, ra	`.ECG_LEAD_OFF_8_CH` [mV]	1	Chest	R3	0.4–5	—	Original only
Precordial ECG v1–v6	`.ELECTROCARDIOGRAM_8_CH` or `.ECG_LEAD_OFF_8_CH` [mV]	500 or 1	Chest (Precordial)	R3	0.4–5	—	Original only
Respiration signals	`.RESPIRATION_3_CH` [RUS]	50	Thoracic, xiphoid, abdominal circumf. straps	R3	0–100	RR, PRQ	Denoising + Peak detection + Quality check + RR
t_1 t_2	`.TEMPERATURE` [°C]	1	Right armpit	R3	34–42 0–60	T_{skin} T_{env}	Data cleaning + Quality check
SpO_2	`.SPO2` [%]	1	Left armpit	R3	90–100	–	Data cleaning + Quality check + Physio. ranges
Acceleration	`.ACCELEROMETER_3D` [m/s^2]	100	Back- mounted	R3	IMU range	–	Original only

Table 4. Original signal-level data dictionary. Each row corresponds to a signal type; each column reports one metadata field for that signal.

The `hr` column stores the HR (beats/min), computed from the electrocardiographic recordings. The `rr` column contains the RR (breaths/min), derived from the respiratory signals. The `spo2` column reports SpO_2 (%). The `T1` and `T2` columns contain the T_{skin} and T_{env} measurements, respectively (°C). Finally, the `Az` column stores the acceleration measured along the direction of the motion of the hand-bike (ms^{-2}).

All variables were derived from the original recordings after the pre-processing and inspection procedures, following the procedure described in the Section Methods.

The `DataTable` explicates the exclusions by inspection reported in Table 8. Therefore, the file presents excluded samples and should therefore be regarded as the author-processed level of the dataset: users who wish to apply different inspection criteria, or to analyze the excluded segments, should start from the original device-processed signals in the `.h5` files, which are released unmodified for all 42 sessions, even for the corrupted acquisitions.

The resulting table provides a compact representation of the synchronized physiological, environmental, and motion-related information collected throughout the monitoring period.

PRQ.mat. The file *PRQ.mat* contains a MATLAB variable named `prq`, which stores PRQ computed throughout the recording sessions. The PRQ is defined as the ratio between HR and RR:

$$\mathrm{PRQ} = \frac{\mathrm{HR}}{\mathrm{RR}} \tag{1}$$

and is therefore a dimensionless quantity describing the relationship between cardiovascular and respiratory activity. PRQ values were computed from the processed HR and RR signals and sampled at a temporal resolution of one value per minute. Consequently, each element of the `prq` variable corresponds to the same one-minute interval used in the `DataTable` contained in `Variable.mat`. The file provides an additional parameter of the extracted HR and RR variables, as described in Section Technical Validation.

Matlab scripts. The Zenodo repository[27] includes three MATLAB scripts that support data visualization, pre-processing, and derivation of physiological variables from the original, device-processed HDF5 recordings.

The script `visualize.m` provides an example workflow for accessing the HDF5 files and visualizing the recorded signals. It loads the electrocardiographic, respiratory, pulse oximetry, temperature, and accelerometer channels, converts the timestamps into human-readable date-time values, and generates representative plots for exploratory analysis and quality assessment.

The script `hr.m` processes the high-resolution electrocardiographic recordings to estimate HR. It applies Butterworth filtering, performs R-peak detection, computes minute-by-minute HR values, and generates a filtered HR time series suitable for longitudinal analyses.

The script `PRQ.m` computes the PRQ, using the variables stored in `Variable.mat`. The script evaluates minute-by-minute PRQ values, calculates descriptive statistics, and provides graphical representations of their temporal evolution and distribution.

Together, these scripts reproduce the main pre-processing and physiological variable extraction procedures described in this work and facilitate reuse of the dataset for further methodological development and comparative analyses.

To facilitate reuse, we list the repository content:

1. *yyyymmdd.zip*: a zip archive containing the session files, named by acquisition date.
2. *.h5 file*: in each session folder a .h5 file is present with the whole device-processed output data recordings.
3. *Variable.mat file*: in each session folder there is a .mat file containing the processed variables, annotated with the samples excluded by inspection.
4. *PRQ.mat file*: in each session folder a .mat file is present with the calculated PRQ feature.
5. *README.txt file*: in which the dataset description and usage is given.

#	Date [dd/mm/yyyy]	Start time [hh:mm:ss]	Duration [hh:mm:ss]	Phase	T_{env}[°C] WeatherSpark	Device model	Bike type	FES	Notes
1	13/01/2024	10:00:00	01:29:36	Race	25–26	Healer R3	Hand-bike	Yes	—
2	09/01/2024	06:00:00	03:10:12	Race	24–25	Healer R3	Hand-bike	Yes	—
3	08/01/2024	07:00:00	01:59:21	Race	24–25	Healer R3	Hand-bike	Yes	—
4	31/12/2023	07:00:00	01:00:40	Race	21–22	Healer R3	Hand-bike	Yes	—
5	30/12/2023	06:00:00	03:24:00	Race	24–25	Healer R3	Hand-bike	Yes	—
6	29/12/2023	08:45:00	02:51:52	Race	24–25	Healer R3	Hand-bike	Yes	—
7	11/12/2023	01:20:00	05:42:45	Train	25–29	Healer R3	Trike	Yes	T_{skin} error
8	27/11/2023	01:27:00	04:13:28	Train	25–29	Healer R3	Trike	Yes	T_{skin} error
9	19/11/2023	06:50:00	02:36:39	Train	25–29	Healer R3	Hand-bike	Yes	T_{skin} error
10	18/11/2023	06:55:00	06:49:42	Train	25–29	Healer R3	Trike	Yes	T_{skin} error
11	05/11/2023	06:40:00	02:13:41	Train	25–29	Healer R3	Trike	Yes	T_{skin} error
12	18/10/2023	08:00:00	01:57:40	Train	25–29	Healer R3	Hand-bike	Yes	T_{skin} error
13	16/10/2023	02:30:00	04:19:56	Train	25–29	Healer R3	Hand-bike	Yes	T_{skin} error
14	15/10/2023	07:40:00	02:30:02	Train	25–29	Healer R3	Hand-bike	Yes	T_{skin} error
15	13/10/2023	15:30:00	01:27:01	Train	30–35	Healer R3	Trike	Yes	T_{skin} error
16	11/10/2023	02:45:00	03:58:30	Train	25–29	Healer R3	Hand-bike	Yes	T_{skin} error
17	09/10/2023	02:40:00	04:31:27	Train	25–29	Healer R3	Trike	Yes	T_{skin} error
18	08/10/2023	07:30:00	02:11:27	Train	25–29	Healer R3	Hand-bike	Yes	T_{skin} error
19	06/10/2023	13:40:00	04:10:27	Train	30–35	Healer R3	Trike	Yes	T_{skin} error
20	05/10/2023	07:30:00	01:55:56	Train	30–32	Healer R3	Hand-bike	Yes	—
21	04/10/2023	03:00:00	04:10:10	Train	30–32	Healer R3	Hand-bike	Yes	—
22	01/10/2023	07:20:00	02:30:19	Train	25–29	Healer R3	Trike	Yes	T_{skin} error
23	29/09/2023	14:00:00	03:22:21	Train	30–35	Healer R3	Hand-bike	Yes	T_{skin} error
24	28/09/2023	07:30:00	01:55:18	Train	25–29	Healer R3	Trike	Yes	T_{skin} error
25	24/09/2023	06:30:00	02:27:25	Train	25–29	Healer R3	Hand-bike	Yes	T_{skin} error
26	12/09/2023	03:40:00	03:21:15	Train	25–29	Healer R3	Trike	Yes	T_{skin} error
27	10/09/2023	07:45:00	02:10:46	Train	25–29	Healer R3	Hand-bike	Yes	T_{skin} error
28	09/09/2023	14:50:00	03:02:05	Train	38–39	Healer R3	Trike	Yes	—
29	08/09/2023	14:40:00	03:54:35	Train	39–40	Healer R3	Hand-bike	Yes	—
30	04/09/2023	03:35:00	03:21:03	Train	33–34	Healer R3	Trike	Yes	—
31	02/09/2023	06:50:00	00:55:13	Train	32–33	Healer R3	Hand-bike	Yes	—
32	01/09/2023	11:30:00	09:16:02	Train	30–35	Healer R3	Hand-bike	Yes	T_{skin} error
33	30/08/2023	03:47:00	03:23:56	Train	31–32	Healer R3	Hand-bike	Yes	—
34	11/08/2023	14:00:00	03:40:19	Train	38–39	Healer R3	Trike	Yes	—
35	27/07/2023	16:47:00	02:48:16	Train	40–41	Healer R3	Trike	Yes	—
36	25/07/2023	21:05:00	08:11:37	Train	37–38	Healer R3	Hand-bike	Yes	—
37	24/07/2023	11:05:00	06:44:06	Train	40–42	Healer R3	Hand-bike	Yes	—
38	23/07/2023	18:00:00	03:23:01	Train	34–36	Healer R3	Trike	Yes	—
39	21/07/2023	10:00:00	03:20:17	Train	36–37	Healer R3	Trike	Yes	—
40	17/07/2023	21:46:00	09:13:11	Train	36–37	Healer R3	Trike	Yes	—
41	15/07/2023	10:00:00	02:51:04	Train	36–37	Healer R3	Trike	Yes	—
42	14/07/2023	15:30:00	02:59:45	Train	37–38	Healer R3	Trike	Yes	—

Table 5. Session-level metadata across the 42 recordings.

6. *function folder*: folder in which all the "getting started" scripts are saved.
7. *visualize.m*: script provides an example workflow for loading the `.h5` recordings and visualizing the acquired physiological signals.
8. *hr.m*: function processes electrocardiographic recordings to derive HR time series.
9. *PRQ.m*: computes the PRQ from the extracted HR and RR signals.
10. *Users Manual Healer.pdf*: Healer device user manual.
11. *metadata.pdf*: a PDF file containing the signal data dictionary and the session-level metadata (Tables 4 and 5).
12. example_A_personalized_GRU.py: pre-trains the GRU model on Sport DB 2.0, fine-tunes it on the HR sessions of this dataset and computes RMSE and cross-correlation on the test sessions (illustrative example A in Data Overview).
13. example_B_temperature_augmentation.py: trains Random Forest, XGBoost and MLP on the SCI cohort with and without the sessions of this dataset and computes the RMSE of the autoregressive temperature forecast on the held-out subjects (illustrative example B in Data Overview).

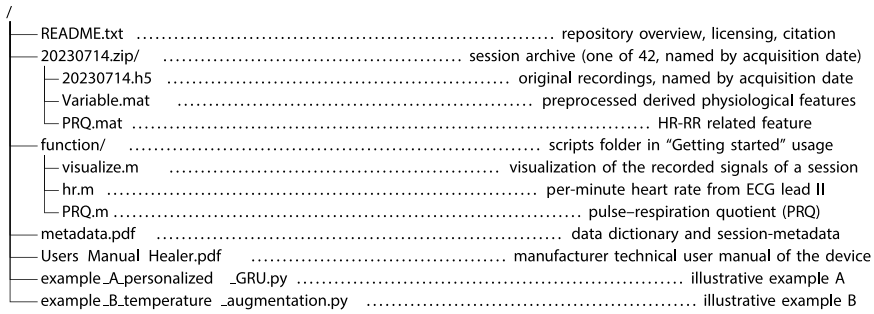

Fig. 5 Folder and file structure overview of the dataset, version v4.0.

Finally, Fig. 5 shows the folder and file structure.

Data Overview

The longitudinal structure of the dataset and the availability of multimodal physiological variables make the resource suitable for methodological reuse in data-driven analyses[46–49]. As proof-of-concept illustrations only – and not as validated clinical tools – we implemented two illustrative modeling workflows. These examples are intended solely to illustrate technical reusability of the dataset; given the single-participant design, results should not be interpreted as evidence of clinical utility or generalizability. In particular, we show: *(i)* a personalized fine-tuning model from longitudinal data; and *(ii)* the use of the proposed dataset as a domain-augmentation resource for skin-temperature predictive modeling in an existing SCI cohort.

A. Personalized GRU model: the first approach develops a Gated Recurrent Unit (GRU)[50] predictive model trained on the publicly available "Sport DB 2.0" dataset[51] and fine-tuned on our data to capture the longitudinal participant-specific HR dynamics. To model the temporal evolution of HR during each exercise session, the model uses the concatenation of the first two sessions as input and the third as the prediction target. We evaluate the average Root Mean Squared Error (RMSE) and the normalized cross-correlation across sessions. The fine-tuned model achieves a mean RMSE of 10.36 beats/min and mean cross-correlation of 0.81, while the pre-trained model achieves a mean RMSE of 21.35 beats/min and a mean cross-correlation equal to 0.40. An example session prediction is shown in Fig. 6(a).
B. Domain-specific data augmentation in predictive modeling: the second approach uses Random Forest (RF), Extreme Gradient Boosting (XGBoost) and Multi-Layer Perceptron (MLP) to forecast the average T_{skin} in subsequent sessions from a few initial observations, applying autoregressive multi-step prediction. The model uses as input the concatenated features of a small number of initial sessions (*n. seed*) and predicts the average temperature of the subsequent session. We compare models trained solely on SCI patients from the dataset by Sánchez-Jiménez *et al.*[52] with models trained on SCI patients plus the additional subject of the proposed dataset. In Fig. 6(b), we show the RMSE between predicted and true mean T_{skin} for the two configurations. In this way, the dataset can serve as a methodological example of domain-specific augmentation, illustrating a possible reuse strategy that would require validation on larger and more heterogeneous SCI cohorts before any clinical application could be considered.

Finally, the Python scripts reproducing the two illustrative examples (*example_A_personalized_GRU.py* and *example_B_temperature_augmentation.py*) are available in the repository, to facilitate reuse. These values are reported only as a proof-of-concept examples for technical reusability.

Technical Validation

The technical validation presented in this section aims to assess the quality and plausibility of both the original recordings and the processed variables. A summary of the main inspection and validation procedures is reported in Table 6, while the corresponding analyses are described in detail in the following subsections.

These derived features are distributed together with the original data to facilitate dataset reuse and reproducibility. Table 7 provides an overview of the physiological variables and derived features included in the dataset. By providing both the original recordings and the processed variables, users can either directly employ the extracted features in statistical analyses and data-driven applications or reproduce the complete processing pipeline starting from the original signals.

Device-level validation. The Healer R3 wearable system used in this study is a certified Class IIa medical device (Medical Device Directive 93/42/EEC, as amended) manufactured by L.I.F.E. Italia S.r.l., compliant with EN ISO 10993-1:2018, EN ISO 14971:2012 (risk management), EN ISO 15223-1:2016, EN 60601-1:2006+A1:2013 and EN 60601-1-2:2015 (general and electromagnetic compatibility requirements for electromedical equipment), EN 60601-1-6:2010+A1:2015 and EN 60601-1-11:2015, EN 60601-2-47:2015 (particular requirements for ambulatory electrocardiographic systems), ISO 80601-2-61:2017 (particular requirements for pulse oximeter equipment), and EN 62304:2006+A1:2015 and EN 62366:2008+A1:2015 (software lifecycle and usability engineering processes).

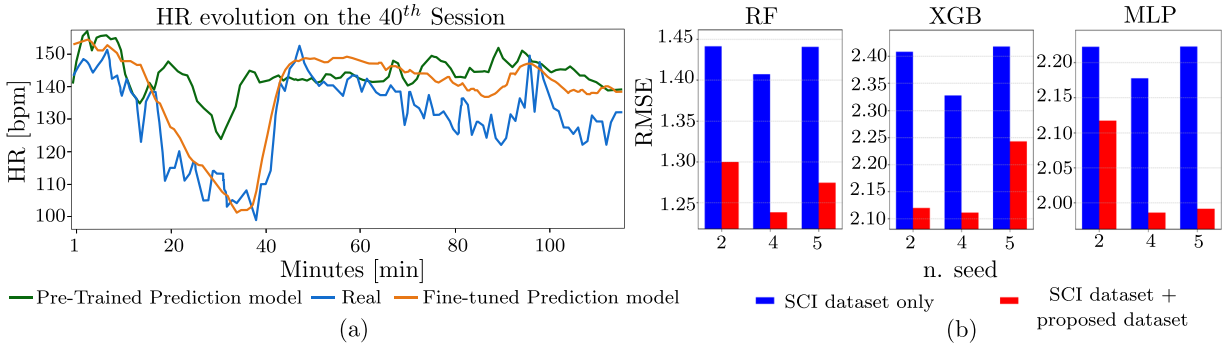

Fig. 6 Proof-of-concept. (a) Predicted HR evolution for the 40th session by the personalized fine-tuned GRU model (RMSE=9.35 beats/min; Corr=0.89) vs pre-trained model (RMSE=20.43 beats/min; Corr=0.49) compared to the real HR trend. The reported model performance refers to one representative session; aggregate performance across all evaluated sessions is reported in the text (b) RMSE evaluation on the models trained with SCI-only dataset and with SCI dataset plus the proposed dataset, as function of *n. seed* and model architecture on the test set.

Analysis	Description
Device-level validation	Sensor calibration, synchronization accuracy and sensor accuracy
Original signals-level validation	Signal quality indices, plausibility of the values, denoising, acquisition completeness, missing data, channel-failure.
PRQ	Ratio between HR and RR
T_{skin}&T_{env}	Discrimination between the recorded axillary/skin temperature and the temperature of the environment
Variables Correlation	HR, RR, z-acceleration, T_{skin} and SpO_2 correlation coefficients analysis
Statistical tests of extracted variables	Variable distributions, physiological relationships, and temporal variability.
Comparison with the state of the art	Comparison of the extracted features with published values to check plausibility.

Table 6. Technical Validation Steps.

Factory calibration and functional testing of the integrated ECG, respiration, temperature, SpO_2, and acceleration sensors are performed by the manufacturer as part of this regulatory certification process. The device technical manual does not describe any user-performed sensor calibration procedure, either at first use or at the start of each recording session. The only operator-side procedure described before an examination is a qualitative visual check of signal adequacy, performed via the Healer Cloud web portal. This check verifies that the acquired signals, and therefore the selected sensorized garment and its adjustments, are adequate; it is not a quantitative calibration against a reference. The sensor calibration is therefore entirely factory-performed and is not repeated by the end user.

Beyond hardware-level calibration, acquired device-processed data are transmitted from the KoR 1 logger and processed through the Healer Software and Healer Cloud platform prior to being made available for analysis. As part of its certified functionality, this platform generates device-level signal-quality indicators along with the native physiological recordings: for example, electrode-skin contact quality (lead-off detection), corresponding to the `.ECG_LEAD_OFF_8_CH` channel group, and the SpO_2 quality, status, perfusion indices (`spo2_quality_eng, spo2_status_eng, spo2_perfusion_eng`). These are the same indices the certified software exposes to the physician for the pre-exam signal-adequacy check described above, and constitute an additional, manufacturer-implemented layer of technical validation upstream of the analyses presented in this work. The internal algorithms and thresholds underlying these manufacturer-side checks are proprietary and were not independently audited by the authors.

According to the technical specifications used in this study, the ECG channels are sampled at 500 Hz with 24-bit A/D; the respiratory mechanics sensors at 50 Hz with 16-bit resolution; the 9-axis Inertial Measurement Unit (IMU) at 100 Hz with 16-bit resolution; and the temperature sensor at 1 Hz with 16-bit resolution. The integrated SpO_2 module has a manufacturer-declared standard accuracy of ± 3% over the 0–100% measurement range at 1 Hz. We note that the manufacturer explicitly labels both the skin temperature and the integrated SpO_2 measurements as estimates not intended for diagnostic use.

All physiological signals were acquired using a common internal hardware clock. This design minimizes inter-channel timing drift across modalities with different native sampling frequencies. For each of the 42 recordings, synchronization was verified by comparing the start/end timestamps of each channel's time vector `.t` within the same session, confirming consistent internal alignment across modalities. Absolute timestamps were referenced to GMT+3, enabling consistent alignment with external data sources (e.g., environmental temperature from the WeatherSpark platform).

Regarding the temperature sensor, the manufacturer specifies a certified working temperature range of 0-40 °C for the device. Since this, the environmental temperatures could possibly affect the temperature-channel malfunction described in Section Methods, alongside the sensor damage explicitly documented for that period.

Parameter	MIN	AVERAGE	MAX
HR [beats/min]	99	139	180
RR [breaths/min]	23	32	40
SpO_2 [%]	90	95	100
T_{skin} [°C]	35	37	39

Table 7. Overview of physiological parameters and derived features.

Signals	Sessions	(a) Acquisition loss	(b) Device malfunction	(c) Quality control exclusion	Inspection rule
ECG (lead II)	42/42	0	0	per session: 0% total: 0%	Window excluded if lead-off flag active, or if clinical assessment by the physicians indicated unreliable signal.
Respiration	42/42	0	0	per session: 0% total: 0%	Window excluded if RR outside physiological range.
T_{skin}	22/42	0	20 sessions; (47.6%)	per session: 28.2 ± 25.7% total: 64.2%	Values outside physiological range; sensor stabilization time
T_{env}	22/42	0	20 sessions; (47.6%)	per session: 9.1 ± 10.0% total: 47.6%	In the remaining sessions, cut the stabilization time as T_{skin} and adjust values according to the WeatherSpark recorded temperature.
SpO_2	42/42	0	0	per session: 13.8 ± 11.8% total: 38.8%	Based on `spo2_quality_eng` or outside physiological range %.
Acceleration (z)	42/42	0	0	per session: 0% total: 0%	None

Table 8. Missing data and exclusions per modality across the 42 recording sessions. Exclusions are separated by cause: (a) acquisition loss and (b) device malfunction are reported at session level, while (c) post-processing exclusions by the inspection rules listed in the last column are in % of the session duration, averaged across all sessions and the total percentage of data excluded on the whole dataset. Original signals in the `.h5` files are released unmodified, including the excluded sessions.

No independent reference-grade device (e.g., clinical 12-lead ECG, calibrated infrared/mercury thermometer, or a reference pulse oximeter) was used in parallel with the Healer system during data collection. Consequently, the sensor accuracy figures reported here reflect manufacturer specifications for the sensor configuration actually used, rather than independent empirical verification by the authors. The full device technical manual is provided alongside the dataset in the Zenodo repository to allow independent verification of all specifications discussed in this section.

Validation of the original signals. This subsection reports acquisition completeness, signal-quality check, and artifact-related aspects of the device-processed physiological recordings across the 42 sessions, combining the certified inspection layer embedded in the Healer acquisition pipeline with independent checks performed by the authors and with continuous clinical oversight of the participant's physiological status.

Regarding the acquisition completeness, dropped samples, and timestamp integrity, the `.h5` files available to the authors are not unprocessed sensor telemetry, but the output of the certified Healer Software/Cloud acquisition and validation pipeline, which handles data transmission from the KoR 1 logger, upload, and internal integrity checks before making recordings available for download.

Acquisition-level artifacts such as transmission packet loss or logger buffer overflows are managed internally by this proprietary pipeline and are not observable by the authors; by design, the architecture—local recording on the KoR 1 logger's internal storage during the session itself, followed by validated upload to Healer Cloud—is intended to prevent the kind of transmission-related data loss that could affect real-time-only acquisition modes. To verify this, for each of the 42 recordings and each signal group we computed the expected number of samples per channel (based on nominal sampling frequency and recorded time span, derived from each channel's own timestamp vector `.t`) and compared it against the number of samples actually present in the delivered files. This analysis showed no dropped samples across the dataset, timestamp continuity consistent with the nominal sampling frequency of each channel, and no missing-data segments attributable to acquisition or transmission loss were found. The only data-quality issues identified in the dataset are those already reported in Section Methods (device malfunction affecting the temperature channel over specific date ranges), rather than acquisition-level dropout.

Table 8 summarizes, for each modality, the number of affected sessions and the percentage of excluded samples by cause.

Consistent with the completeness analysis above, no acquisition channel-level failures were identified.

As previously mentioned, being a certified medical device, the Healer system intrinsically embeds its own signal-quality assessment as part of its manufacturer-validated acquisition pipeline, rather than requiring the authors to define post-hoc, independent quality-scoring thresholds. For SpO_2, this is reflected in the device-native quality, status, perfusion channels—`spo2_quality_eng`, `spo2_status_eng`, and `spo2_perfusion_eng`—already present among the original dataset fields, consistent with the exclusion criteria described in Section Methods.

For ECG, the `.ECG_LEAD_OFF_8_CH` channel group provides the device's own electrode-skin contact quality estimate (lead-off detection)—the same certified signal-verification functionality that

Healer Cloud exposes to the physician before starting an exam. We consider these device-native indices a manufacturer-validated, ready-to-use layer of signal-quality assessment already embedded in the delivered dataset, and did not derive independent quality metrics for these two modalities.

As further quality check, ECG noise segments and motion artifacts were smoothed following the filtering and denoising procedure already described in Section Methods, based on a second-order Butterworth bandpass filter (4-20Hz), consistent with widely adopted, robust, and reproducible approaches in physiological signal processing.

Even if manually annotated or device reference annotations were not collected or stored for this dataset, we quantitatively compared the R-peaks identification from the filtered lead II signal using the multiple validated detection tools already cited in Section Methods. The agreement of our processing with these comparative tools[39,40], on average across them, was quantified with the following measures.

1. Over all beats detected in the 42 sessions, 98.56% of the R-peaks of our detector were matched by the tools, with a median timing difference of 4.87 ms within a 150 ms tolerance.
2. The HR from the detectors differed from ours by 2 bpm on average compared to our method.

These results were used as an internal consistency check on peak-detection quality, consistent with the literature[8,53–55], alongside the visual inspection of the clinical team.

However, the agreement between R-peak detection methods is not meant to be a validation against a ground truth, but as inter-method agreement on the same device-output signal, and does not measure detection accuracy, since no reference ECG or manual annotation is available, and the errors shared by all detectors cannot be revealed.

Since no gold-standard reference signal was available, ectopic-beat handling relied on clinical supervision during the study rather than on retrospective manual annotation. As mentioned, all training sessions and the endurance race were planned and supervised by the clinical team of VBRRII, who monitored the participant's physiological status daily – including data transmitted from the FES device – throughout the entire seven-month period (training and subsequent race). No cardiac arrhythmia, ectopic activity, or other physiologically relevant anomaly were reported by the clinical team over the course of the study.

For respiration, temperature, and acceleration, as for the ECG channel, physiological plausibility was continuously monitored throughout the study by the VBRRII clinical team. Sensor specifications for these modalities—accuracy, resolution, and sampling frequency—are documented in the manufacturer's technical manual. For respiration and acceleration, no physiologically anomalous readings were reported by the clinical team over the course of the study, and no dedicated plausible-range flagging beyond this clinical oversight was therefore necessary. Temperature is the only exception among the three modalities: given the device malfunction already reported, an explicit physiological-range check (34-42 °C) was applied specifically to this channel to identify and remove implausible values, complementing the clinical oversight rather than substituting it. We further clarify that the temperature-stabilization exclusion criterion—removal of segments recorded immediately after sensor-skin contact, before the reading had stabilized—was defined empirically by the authors based on visual inspection of the temperature traces, as the manufacturer's technical manual does not specify a recommended sensor stabilization time.

The Pulse-Respiration Quotient. The relationship between HR and RR was examined through PRQ, defined as HR/RR[56]. Both HR and RR increase with exercise, and their ratio has been reported to vary with physical load[57]. In the literature, PRQ values between 2 and 10 have been reported in male subjects, with values of about 4–5 under resting conditions[56,57]. PRQ has been used, for example, to characterize the response to the transition from the supine to the standing position, in which it generally increases depending on the efficiency of orthostatic cardiovascular regulation[56]; this application is reported here only as background and was not investigated in the present dataset.

Figure 7 shows the distribution of PRQ (f-PRQ) for each recording session (gray lines) and their mean (black line). The distributions are similar across sessions, and their peaks lie at values of about 4–5. HR and RR are derived from two independent sensing channels; the resulting PRQ values fall within the range reported in the literature, which is consistent with, but does not validate, the extraction of the two variables. No reference values of PRQ exist for individuals with SCI, in whom autonomic and respiratory control can be altered by the level and completeness of the lesion. PRQ is therefore provided as a derived variable for exploratory reuse, for example in studies of cardiorespiratory coupling, and not as an indicator of the participant's status.

Inspection and adjustment of temperature channels. T_{skin} and T_{env} were simultaneously acquired through independent sensing channels embedded in the wearable system, referred to as *t1* and *t2*, respectively. Although recorded separately, prolonged measurements under dynamic conditions could introduce coupling between the signals due to sensor proximity or local microenvironment effects. To ensure plausible interpretation, we visually inspected both T_{skin} and T_{env} to identify systematic offsets, drifts, and potential inconsistencies.

To gauge the plausibility of *t2*, we compare the recorded signal with external environmental data, T_{site}, from the WeatherSpark monitoring platform. The information about environmental temperatures in the relevant regions of Saudi Arabia is available at https://weatherspark.com, which provides an external reference for plausibility. We use the T_{site} values to systematically rescale the *t2* traces, effectively saturating them within a physically consistent range defined by T_{site}.

Subsequently, we re-evaluate ΔT to verify that it remains physiologically consistent with expected thermoregulatory responses. We constrain *t1* values within established human physiological limits (34–42 °C) and exclude signal segments identified as implausible, artifact-corrupted, or exhibiting abrupt non-physiological transitions using statistical thresholding based on distribution analysis.

The pseudocode of the pre-processing pipeline is reported in the following Algorithm 1.

To provide a clearer distinction between original (device-processed output) and corrected data, we provide T_{site} ranges of each experimental session in the session-level metadata Table 5. The original signals *t1* and *t2* are uploaded in the `.h5` file, while the corresponding processed T_{skin} alongside the T_{env} signals are provided in the repository in the `Variable.mat` file, allowing users to perform further analyses. We also state that the performed processing was applied to the entire dataset, including all signals from all available sessions, except for the sessions affected by device malfunction and the excluded samples reported in Table 8.

The consistency of the temperature measurements and the relationship between T_{skin} and T_{env} can be examined in the context of physiological ranges and trends reported in previous studies[16–20]. From our preliminary analysis, the measurements exhibit physiologically plausible relationships between T_{skin} and T_{env} supporting the plausibility of both the acquired signals and the derived variables.

Finally, we stress that the applied correction was intended to improve plausibility. Since the corrected T_{env} is constrained to the reference range by construction, its agreement with T_{site} provides no evidence of the effective accuracy of the sensor. Original *t2* data is preserved in the dataset repository.

Algorithm 1 Processing of the temperature channels, applied to each recording session s_i.

Require: $s = \{s_1, \dots, s_{42}\}$: recording sessions;
for each session:
$t1(k)$, $t2(k)$, $k = 1, \dots, K$: original temperature signals sampled at $f_s = 1$ Hz;
$k_s = T_{stab} \cdot f_s + 1$: first sample after sensor stabilization, with $T_{stab} \approx 10$ min;
$[T_{site}^{min}, T_{site}^{max}]$: range of the air temperature during the session (WeatherSpark).
Ensure: for each session:
$T_{skin}(k)$: skin temperature after inspection;
$T_{env}(k) \in [T_{site}^{min}, T_{site}^{max}]$: $t2(k)$ corrected environmental temperature;
$\Delta T(k)$: channel difference before correction;
$\Delta T(k)^{adj}$: channel difference after correction;
c, a: offset and scale factor;

for $i = 1, \dots, 42$ **do** ▷ all quantities refer to session s_i
  if s_i is affected by the sensor malfunction **then**
    $T_{skin}(k), T_{env}(k), \Delta T(k) \leftarrow$ NaN for all k ▷ device malfunction
  else
  Step 1 – Axillary skin temperature
    $T_{skin}(k) \leftarrow$ NaN for $k < k_s$; $T_{skin}(k) \leftarrow t1(k)$ for $k \geq k_s$ ▷ sensor stabilization
    for $k = k_s, \dots, K$ **do**
      if $T_{skin}(k) < 34$ °C **or** $T_{skin}(k) > 42$ °C **then**
        $T_{skin}(k) \leftarrow$ NaN ▷ plausibility range
      end if
    end for
  Step 2 – Environment Temperature
    $T_{env}(k) \leftarrow$ NaN for $k < k_s$; ▷ sensor stabilization
    $T_{env}(k) \leftarrow t2(k)$ for $k \geq k_s$;
  Step 3 – Mapping of $T_{env}(k)$ into the reference range
    $\Delta T(k) \leftarrow T_{env}(k) - T_{skin}(k)$ ▷ original channel difference
    $T_{env}^{lo}, T_{env}^{hi} \leftarrow$ 1st and 99th percentiles of T_{env}
    $m_{site} \leftarrow (T_{site}^{min} + T_{site}^{max})/2$; $m_{T_{env}} \leftarrow (T_{env}^{lo} + T_{env}^{hi})/2$
    if $T_{env}^{hi} - T_{env}^{lo} \leq T_{site}^{max} - T_{site}^{min}$ **then**
      $a \leftarrow 1$ ▷ shift only
    else
      $a \leftarrow \dfrac{T_{site}^{max} - T_{site}^{min}}{T_{env}^{hi} - T_{env}^{lo}}$ ▷ range compression
    end if
    $c \leftarrow m_{site} - a\, m_{T_{env}}$ ▷ affine offset
    for $k = k_s, \dots, K$ **do**
      $T_{env}(k) \leftarrow c + a\, T_{env}(k)$ ▷ $= T_{env}(k) + c$ when $a = 1$
      if $T_{env}(k) \notin [T_{site}^{min}, T_{site}^{max}]$ **then**
        $T_{env}(k) \leftarrow \min\big(\max(T_{env}(k), T_{site}^{min}), T_{site}^{max}\big)$; ▷ saturation
      end if
    end for
    $\Delta T^{adj}(k) \leftarrow T_{env}(k) - T_{skin}(k)$ ▷ change after correction
  end if
  store T_{skin}, T_{env}, ΔT, c, a, ΔT^{adj} of session s_i
end for

Correlation of the extracted variables in frequency domain. The assessment of relationships among independently acquired physiological variables provides an additional consistency check. Several physiological parameters included in the dataset are expected to exhibit coordinated variations during physical activity, as

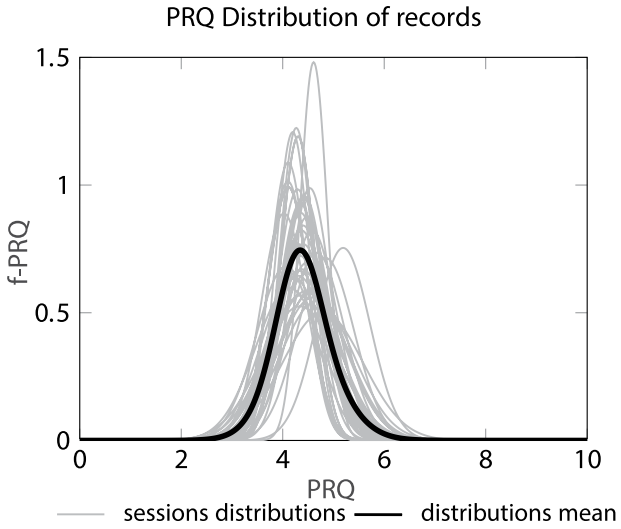

Fig. 7 Distribution of PRQ values. Individual sessions are shown in light gray, with the mean distribution in black.

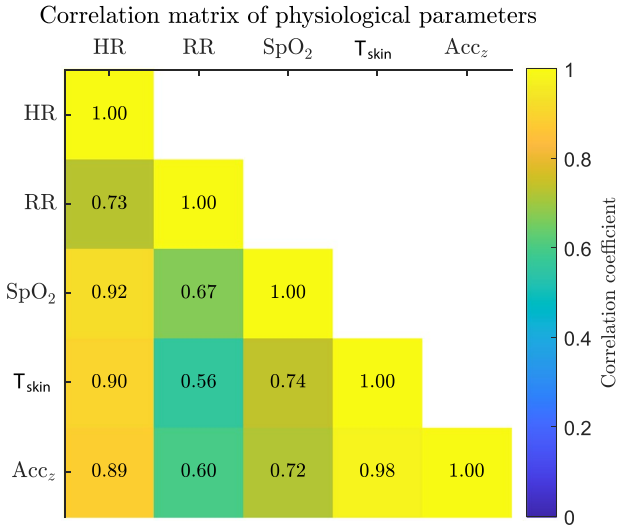

Fig. 8 Heatmap of the pairwise correlation coefficients among the considered frequency-domain physiological variables.

reported in previous studies. For example, HR and RR are both influenced by metabolic demand and have been shown to vary concurrently during exercise and stress conditions[58]. Similar interactions may be expected among T_{skin}, SpO_2, and motion-related measurements.

We compared the variables in the frequency domain, within each recording session. First, all variables were brought to the time base of HR, i.e., one value per minute: SpO_2, T_{skin} and Acc_z were downsampled to the HR samples with an anti-aliasing filter. After removing the session mean, we estimated Power Spectral Density (PSD) of each variable over the whole session with Welch's method with default settings: Hamming window, eight segments with 50% overlap, 256-point FFT, 129 frequency bins. With one sample per minute, the PSD spans 0–0.5 cycles/min, i.e., fluctuations with periods longer than 2 min. For each pair of variables, we computed the Pearson correlation coefficient between the two PSDs over the 129 frequency bins (r_{PSD}), separately for each session, and we report its mean across the number of sessions in Fig. 8. A high r_{PSD} indicates that two variables distribute their power similarly across these slow frequencies. Since PSD discards phase information, it does not indicate that the two variables vary at the same time. This analysis is therefore distinct from the session-level statistics of the following subsection, where statistical tests are computed between session-averaged values across sessions in time domain.

To evaluate the consistency of the recorded signals and derived variables, variations of HR, RR, z-axis acceleration, T_{skin}, and SpO_2 were investigated. The analysis was performed by computing correlation coefficients between the spectral representations of each variable pair. The resulting coefficients provide a coarse, descriptive

Physiological parameter	Our Work	Abel *et al.*[21]	Abel *et al.*[22]	Chou *et al.*[20]	Hertig *et al.*[18]	Galan *et al.*[16]	Yamasaki *et al.*[17]
HR [beats/min]	139 ± 21	146 ± 23	137 ± 20	152 ± 30	126 ± 34	181 ± 9(1)	–
RR [breaths/min]	32 ± 4.83	–	–	–	–	–	–
SpO_2 [%]	95.20 ± 2.49	–	–	–	–	–	–
T_{body}/T_{skin} [°C]	36.88 ± 0.67	–	38.8 ± 2.4(2)	37 ± 1.9	37.7 ± 0.37	36 ± 1.97	37.5 ± 1
T_{env} [°C]	30.52 ± 5.41	–	21 ± 1	27 ± 15	21 ± 1	–	28 ± 5

Table 9. Comparison of the physiological values obtained in our experiment with the state of the art. (1) Retrieved from HR peak. (2)Rectal temperature.

check of the plausibility of the multimodal recordings. Since they are computed on repeated sessions of a single participant, they should not be considered as population-level evidence.

Figure 8 shows the correlation matrix among the considered physiological variables. Since correlation matrices are symmetric by definition, only the lower triangular part is displayed. The color intensity reflects the magnitude of the correlation coefficients, allowing a more immediate comparison among the pairwise associations.

Statistical tests of extracted variables. To determine the most appropriate statistical test for analyzing the relationships among variables (e.g., parametric *vs* non-parametric), we first assessed their distributions. Contrary to the previous section, which was performed in the frequency domain and phase-agnostic, this analysis was performed in the temporal domain.

Here, we set significance level of 0.05, since smaller values of α make rejection harder, reducing the risk of false conclusions. To assess the relationships among the physiological variables, the minute-by-minute observations were first aggregated at the session level. Specifically, for each recording session, the mean value of each variable was calculated over the corresponding session, resulting in one representative observation per session and variable. Pairwise associations among variables were then evaluated across the resulting session-level observations. All statistical tests were performed on session-level means, so that the recording session is the statistical unit (42, or 22 for the pairs involving T_{skin}). Sessions are observations of the same participant and are not independent: the coefficients describe within-participant co-variation across sessions, and not independent or population-level evidence.

First, we assess the distribution of session-averaged variables using the Shapiro–Wilk test[59], whose null hypothesis is data following a normal distribution (*normality hypothesis*). This test computes a parameter $W \in [0, 1]$, where values closer to 1 indicate a closer agreement with a normal distribution. The normality hypothesis could not be rejected for HR ($W = 0.975$, $p = 0.235$), RR ($W = 0.968$, $p = 0.116$), T_{env} ($W = 0.946$, $p = 0.106$), and T_{skin} ($W = 0.956$, $p = 0.103$), whereas SpO_2 ($W = 0.920$, $p = 0.0007$) and Acc_z ($W = 0.923$, $p = 0.0009$) deviated from normality. Note that the T_{env} values result from the correction described in Algorithm 1, which maps each session onto the air-temperature range of the acquisition site; their distribution therefore reflects this reference rather than the original data.

Since not all variables are normally distributed, non-parametric methods are adopted throughout, as they make no assumptions on the data distribution.

For the relationships among variables, we use the Spearman's rank correlation coefficient ρ[60], a non-parametric measure of monotonic association between two variables that is robust to non-normal distributions and outliers. Its measure ρ ranges from -1 to $+1$: values near $+1$ indicate a positive monotonic relationship, values near -1 indicate a negative one, and values near 0 indicate little or no monotonic association. We observed positive associations between HR and SpO_2 ($\rho = 0.391$, $p = 0.011$ over 42 sessions), and between T_{skin} and Acc_z ($\rho = 0.471$, $p = 0.027$ over 22 sessions, due to corrupted T_{skin} records). We did not perform any statistical analysis between T_{skin} and T_{env}, since T_{skin} partially depends on T_{env} after the correction process described in Algorithm 1.

Comparison with the state of the art. To assess the plausibility of the derived physiological variables, the distributions and ranges observed in the dataset were compared with values reported in previous studies (see Table 1) involving individuals with SCI during endurance exercise. As summarized in Table 9, the HR measurements fall within ranges previously reported in the literature. Similarly, the recorded T_{skin} and T_{env} profiles are consistent with observations from comparable exercise and monitoring protocols. Although direct comparisons are inherently limited by differences in study design, sensor configurations, and acquisition procedures, the overall agreement with published data supports that the recorded values fall within the ranges reported in the literature, which indicates their physiological plausibility.

Limitations. This dataset was collected from a single participant with paraplegia under a specific longitudinal protocol and therefore does not capture the variability associated with different injury characteristics, levels of physical conditioning, or physiological responses across the broader SCI population. As an N-of-1 dataset, it does not support statistical generalization, population-level inference, or direct clinical decision-making. Any predictive or clinical application illustrated in this work is exploratory and requires independent validation on larger, demographically and clinically diverse cohorts before translation into rehabilitation or clinical practice. Users should treat the dataset as a resource for hypothesis generation, longitudinal single-subject modeling, and methodological/signal-processing benchmarking.

Beyond the single-participant design already discussed above, the released dataset lacks certain session-level metadata that could further support physiological modeling and contextual interpretation: GPS-derived route,

distance, and altitude information; FES signals; and structured per-session logs of rest periods, workload, power output, speed, slope, humidity, perceived exertion, hydration status, sleep, nutrition, medication, or clinical status beyond the general supervision already described. These fields were not part of the acquisition or record-keeping configuration adopted during this study and cannot be reliably reconstructed retrospectively.

We also state that no reference ECG device and manually annotated subset were recorded simultaneously with the Healer R3. The quantitative evaluation of R-peak detection reported in Technical Validation therefore measures the agreement between independent detection tools on the same device-output signals and the clinical assessment, not the accuracy against a ground truth.

The dataset was acquired under a specific longitudinal protocol combining structured para-handcycling training and endurance competition. As a result, the recordings reflect the physiological and environmental conditions experienced by this participant and should not be considered representative of all individuals with SCI or all rehabilitation settings.

Comparison with previously published datasets may also be challenging because of differences in sensor configurations, acquisition protocols, monitored variables, and recording durations.

Usage Notes

The scripts supporting data access, visualization, and feature extraction are deposited together with the dataset in the Zenodo repository (DOI: https://doi.org/10.5281/zenodo.23168228)[27].

A full description is provided in Section Data Records. To ensure correct execution, the scripts should be placed in the same directory as the corresponding data files and run using MATLAB software. The accompanying MATLAB scripts were developed and tested in MATLAB R2023b, that require the Signal Processing Toolbox and the Statistics and Machine Learning Toolbox.

Samples excluded by inspection are annotated in `Variable.mat` and `PRQ.mat`. Users who wish to apply different inspection criteria, to analyze excluded segments or to process the data independently should start from the original device-processed signals in the `.h5` files, which are released unmodified for all 42 sessions.

Data availability

The complete dataset described in this study is publicly available in the Zenodo repository with https://doi.org/10.5281/zenodo.23168228 with Creative Commons Attribution 4.0 International (CC BY 4.0) license. Please cite version v4.0 of the repository[27]. The repository contains the device-processed physiological recordings, derived physiological variables and the PRQ evaluation, alongside the device manual provided by the manufacturer, added in the repository. All files are openly accessible without restrictions under the terms specified in the repository record.

Code availability

Alongside the methods presented here, the code used for signal pre-processing and computation of physiological variables is publicly available as part of the Zenodo repository associated with this dataset at the following link https://doi.org/10.5281/zenodo.23168228. In detail, the repository includes the *visualize.m* script to open the .h5 device output data file and visualize the signal waveforms. The *PRQ.m* and *hr.m* functions evaluate the PRQ and the ECG signals filtering along with the HR values, respectively. Moreover, the Python scripts reproducing the two illustrative examples (*example_A_personalized_GRU.py* and *example_B_temperature_augmentation.py*) are available in the latest version v4.0 of the repository. No restrictions apply to access or reuse beyond those specified in the repository license. The exact version v4.0 of the code and data used in this study is archived in the corresponding Zenodo release.

Received: 19 June 2026; Accepted: 28 October 2026;
Published: xx xx xxxx

References

1. Bernhard, M., Gries, A., Kremer, P. & Böttiger, B. W. Spinal cord injury (SCI)—prehospital management. *Resuscitation* **66**, 127-139 https://doi.org/10.1016/j.resuscitation.2005.03.005 (2005).
2. Ahuja, C. S. *et al.* Traumatic spinal cord injury. *Nat. Rev. Dis. Primers* **3**, 1–21 https://doi.org/10.1038/nrdp.2017.18 (2017).
3. Bromley, I.Tetraplegia and Paraplegia: A Guide for Physiotherapists https://doi.org/10.1016/B978-0-443-10180-9.X5001-3 (Elsevier Health Sciences, 2006).
4. Fong, S., Hang, Y., Mohammed, S. & Fiaidhi, J. Stream-based biomedical classification algorithms for analyzing biosignals. *J. Inf. Process. Syst.* **7**, 717 https://doi.org/10.3745/JIPS.2011.7.4.717 (2011).
5. Mohammed, K. I. *et al.* Real-time remote-health monitoring systems: a review on patients prioritisation for multiple-chronic diseases, taxonomy analysis, concerns and solution procedure. *J. Med. Syst.* **43**, 1–21 https://doi.org/10.1007/s10916-019-1362-x (2019).
6. Khaparkar, S. & Mishra, A. A smart tele-healthcare system for real-time health monitoring and remote consultation. In *2023 1st International Conference on Innovations in High Speed Communication and Signal Processing (IHCSP)* 57–62 (2023). https://doi.org/10.1109/IHCSP56702.2023.10127169
7. Ahmed, S. *et al.* Noncontact assessment for fatigue based on heart rate variability using IR-UWB radar. *Sci. Rep.* **12**, 14211 https://doi.org/10.1038/s41598-022-18498-w (2022).
8. Task Force of the European Society of Cardiology and the North American Society of Pacing and Electrophysiology. Heart rate variability: standards of measurement, physiological interpretation, and clinical use. *Circulation* **93**, 1043–1065 https://doi.org/10.1161/01.CIR.93.5.1043 (1996).
9. Mohanavelu, K., Lamshe, R., Poonguzhali, S., Adalarasu, K. & Jagannath, M. Assessment of human fatigue during physical performance using physiological signals: a review. *Biomed. Pharmacol. J.* **10**, 1887–1896 https://doi.org/10.13005/bpj/1308 (2017).
10. Halomoan, J., Ramli, K., Sudiana, D., Gunawan, T. S. & Salman, M. ECG-based driving fatigue detection using heart rate variability analysis with mutual information. *Information* **14**, 539 https://doi.org/10.3390/info14100539 (2023).
11. Jäkel, B. *et al.* Hand grip strength and fatigability: correlation with clinical parameters and diagnostic suitability in ME/CFS. *J. Transl. Med.* **19**, 1–12 https://doi.org/10.1186/s12967-021-02774-w (2021).

12. Wang, F., Wang, H. & Fu, R. Real-time ECG-based detection of fatigue driving using sample entropy. *Entropy* **20**, 196 https://doi.org/10.3390/e20030196 (2018).
13. Fischer, G., Figueiredo, P. & Ardigò, L. P. Bioenergetics and biomechanics of handcycling at submaximal speeds in athletes with a spinal cord injury. *Sports* **8**, 16 https://doi.org/10.3390/sports8020016 (2020).
14. Stephenson, B. T., Stone, B., Mason, B. S. & Goosey-Tolfrey, V. L. Physiology of handcycling: a current sports perspective. *Scand. J. Med. Sci. Sports* **31**, 4–20 https://doi.org/10.1111/sms.13835 (2021).
15. Kraaijenbrink, C. *et al*. Biophysical aspects of handcycling performance in rehabilitation, daily life and recreational sports; a narrative review. *Disabil. Rehabil.* **43**, 3461–3475 https://doi.org/10.1080/09638288.2020.1815872 (2021).
16. Galan-Carracedo, J., Suarez-Segade, A., Guerra-Balic, M. & Oviedo, G. R. The dynamic and correlation of skin temperature and cardiorespiratory fitness in male endurance runners. *Int. J. Environ. Res. Public Health* **16**, 2869 https://doi.org/10.3390/ijerph16162869 (2019).
17. Yamasaki, M. *et al*. Characteristics of body heat balance of paraplegics during exercise in a hot environment. *J. Physiol. Anthropol. Appl. Human Sci.* **20**, 227–232 https://doi.org/10.2114/jpa.20.227 (2001).
18. Hertig-Godeschalk, A. & Perret, C. How elite athletes with a spinal cord injury sweat during exercise—an exploratory study. *Sports* **12**, 81 https://doi.org/10.3390/sports12030081 (2024).
19. Kenny, G. P. & McGinn, R. Restoration of thermoregulation after exercise. *J. Appl. Physiol.* **122**, 933–944 https://doi.org/10.1152/japplphysiol.00517.2016 (2017).
20. Chou, T.-H. & Coyle, E. F. Cardiovascular responses to hot skin at rest and during exercise. *Temperature* **10**, 326–357 https://doi.org/10.1080/23328940.2022.2109931 (2023).
21. Abel, T., Burkett, B., Schneider, S., Lindschulten, R. & Strüder, H. K. The exercise profile of an ultra-long handcycling race: the Styrkeprøven experience. *Spinal Cord* **48**, 894–898 https://doi.org/10.1038/sc.2010.40 (2010).
22. Abel, T., Schneider, S., Platen, P. & Strüder, H. K. Performance diagnostics in handbiking during competition. *Spinal Cord* **44**, 211–216 https://doi.org/10.1038/sj.sc.3101845 (2006).
23. Ganesh, S. & Mishra, C. Physical activity and quality of life among adults with paraplegia in Odisha, India. *Sultan Qaboos Univ. Med. J.* **16**, e54 https://doi.org/10.18295/squmj.2016.16.01.010 (2016).
24. Störmer, S. *et al*. Chronic pain/dysaesthesiae in spinal cord injury patients: results of a multicentre study. *Spinal Cord* **35**, 446–455 https://doi.org/10.1038/sj.sc.3100411 (1997).
25. Nene, A. V., Hermens, H. J. & Zilvold, G. Paraplegic locomotion: a review. *Spinal Cord* **34**, 507–524 https://doi.org/10.1038/sc.1996.94 (1996).
26. Krakowska, N. *et al*. Rehabilitation of patients with paraplegia—a review of the diversity of forms. *J. Educ. Health Sport* **9**, 534–546 https://doi.org/10.5281/zenodo.3235989 (2019).
27. Spinazzola, E. & Prono, L. A longitudinal and multimodal physiological signals dataset of para handcycling training and race for SCI rehabilitation (Version v4.0). Zenodohttps://doi.org/10.5281/zenodo.23168228 (2026).
28. Wilkinson, M. D. *et al*. The FAIR guiding principles for scientific data management and stewardship. *Sci. Data* **3**, 1–9 https://doi.org/10.1038/sdata.2016.18 (2016).
29. L.I.F.E Italia Srl. https://italchamber.qc.ca/companies/l-i-f-e-italia-srl/.
30. Jin, B. *et al*. A simple device to illustrate the Einthoven triangle. *Biophys. J.* **102**, 211a https://doi.org/10.1152/advan.00029.2012 (2012).
31. Peper, E., Groshans, G. H., Johnston, J., Harvey, R. & Shaffer, F. Calibrating respiratory strain gauges: what the numbers mean for monitoring respiration. *Biofeedback* **44**, 101–105 https://doi.org/10.5298/1081-5937-44.2.06 (2016).
32. Mirmohamadsadeghi, L. & Vesin, J.-M. Respiratory rate estimation from the ECG using an instantaneous frequency tracking algorithm. *Biomed. Signal Process. Control* **14**, 66–72 https://doi.org/10.1016/j.bspc.2014.07.003 (2014).
33. Chan, E. D., Chan, M. M. & Chan, M. M. Pulse oximetry: understanding its basic principles facilitates appreciation of its limitations. *Respir. Med.* **107**, 789–799 https://doi.org/10.1016/j.rmed.2013.02.004 (2013).
34. Appathurai, A. *et al*. A study on ECG signal characterization and practical implementation of some ECG characterization techniques. *Measurement* **147**, 106384 https://doi.org/10.1016/j.measurement.2019.02.040 (2019).
35. Spinazzola, E., Prono, L., Pareschi, F., Rovatti, R. & Setti, G. A simple approach to ECG motion artifacts reduction by MDWD coefficients removal. In *2025 IEEE International Symposium on Circuits and Systems (ISCAS)* 1–5 https://doi.org/10.1109/ISCAS56072.2025.11043932 (2025).
36. Menaceur, N. E., Kouah, S. & Derdour, M. Adaptive filtering strategies for ECG signal enhancement: a comparative study. In *2024 6th International Conference on Pattern Analysis and Intelligent Systems (PAIS)* 1–6 https://doi.org/10.1109/PAIS62114.2024.10541144 (2024).
37. Malik, M. *et al*. Heart rate variability: standards of measurement, physiological interpretation, and clinical use. *Eur. Heart J.* **17**, 354–381 (1996).
38. AL-Ziarjawey, H. A. J. & çankaya, I. Heart rate monitoring and PQRST detection based on graphical user interface with Matlab. *Int. J. Inf. Electron. Eng.* **5**, 311 https://doi.org/10.7763/IJIEE.2015.V5.550 (2015).
39. de Carvalho, J. L. A., da Rocha, A. F., de Oliveira Nascimento, F. A., Neto, J. S. & Junqueira, L. F. Development of a Matlab software for analysis of heart rate variability. In 6th International Conference on Signal Processing, 2002 Vol. 2, 1488–1491 (2002). https://doi.org/10.1109/ICOSP.2002.1180076
40. Vollmer, M. HRVTool—an open-source Matlab toolbox for analyzing heart rate variability. In 2019 Computing in Cardiology (CinC) 1–4 (2019). https://doi.org/10.22489/CinC.2019.032
41. Charlton, P. H. *et al*. Breathing rate estimation from the electrocardiogram and photoplethysmogram: a review. *IEEE Rev. Biomed. Eng.* **11**, 2–20 https://doi.org/10.1109/RBME.2017.2763681 (2017).
42. Leube, J. *et al*. Reconstruction of the respiratory signal through ECG and wrist accelerometer data. *Sci. Rep.* **10**, 14530 https://doi.org/10.1038/s41598-020-71539-0 (2020).
43. Nicolò, A., Massaroni, C., Schena, E. & Sacchetti, M. The importance of respiratory rate monitoring: from healthcare to sport and exercise. *Sensors* **20**, 6396 https://doi.org/10.3390/s20216396 (2020).
44. Carey, D. G., Schwarz, L. A., Pliego, G. J. & Raymond, R. L. Respiratory rate is a valid and reliable marker for the anaerobic threshold: implications for measuring change in fitness. *J. Sports Sci. Med.* **4**, 482 (2005).
45. Migliaccio, G. M., Russo, L., Maric, M. & Padulo, J. Sports performance and breathing rate: what is the connection? A narrative review on breathing strategies. *Sports* **11**, 103 https://doi.org/10.3390/sports11050103 (2023).
46. Che, Z., Purushotham, S., Cho, K., Sontag, D. & Liu, Y. Recurrent neural networks for multivariate time series with missing values. *Sci. Rep.* **8**, 1–12 https://doi.org/10.1038/s41598-018-24271-9 (2018).
47. Spinazzola, E. *et al*. Motion tracking for automatically controlled functional electrical stimulation system in mirror therapy configuration: the enhanced Lazarus solution. *IEEE Access* **13**, 148992–149009 https://doi.org/10.1109/ACCESS.2025.3600583 (2025).
48. Mahmoud, Y., Horvath, K. & Zhou, Y. Deep learning for predicting rehabilitation success: advancing clinical and patient-reported outcome modeling. *Electronics* **14**, 1082 https://doi.org/10.3390/electronics14061082 (2025).
49. Trabassi, D. *et al*. Optimizing rare disease gait classification through data balancing and generative AI: insights from hereditary cerebellar ataxia. *Sensors* **24**, 3613 https://doi.org/10.3390/s24113613 (2024).

50. Ławryńczuk, M. & Zarzycki, K. LSTM and GRU type recurrent neural networks in model predictive control: a review. *Neurocomputing* **632**, 129712 https://doi.org/10.1016/j.neucom.2025.129712 (2025).
51. Burattini, L.*et al*. Sport DB 2.0. *Mendeley Data, V1* https://doi.org/10.17632/kzkjkt7mx2.1 (2023).
52. Sanchez-Jimenez, J. L., Aparicio-Aparicio, I. & Priego-Quesada, J. I. Dataset of effect of spinal cord injury on the skin temperature of different regions of interest during a graded exercise test in a moderate temperature environment. *Mendeley Data, V1* (2024). https://doi.org/10.17632/2z2d5wvy43.1
53. Association for the Advancement of Medical Instrumentation. ANSI/AAMI EC13:2002/(R)2007 – Cardiac monitors, heart rate meters, and alarms (AAMI, Arlington, VA, 2002).
54. Pan, J. & Tompkins, W. J. A real-time QRS detection algorithm. *IEEE Trans. Biomed. Eng.* **BME-32**, 230–236 https://doi.org/10.1109/TBME.1985.325532 (1985).
55. Köhler, B.-U., Hennig, C. & Orglmeister, R. The principles of software QRS detection. *IEEE Eng. Med. Biol. Mag.* **21**, 42–57 https://doi.org/10.1109/51.993193 (2002).
56. Scholkmann, F. & Wolf, U. The pulse-respiration quotient: a powerful but untapped parameter for modern studies about human physiology and pathophysiology. *Front. Physiol.* **10**, 371 https://doi.org/10.3389/fphys.2019.00371 (2019).
57. Hildebrandt, G. & Daumann, F.-J. Die Koordination von Puls- und Atemrhythmus bei Arbeit. *Int. Z. Angew. Physiol. Einschl. Arbeitsphysiol.* **21**, 27–48 https://doi.org/10.1007/BF00693386 (1965).
58. Weise, F., Heydenreich, F., Kropf, S. & Krell, D. Intercorrelation analyses among age, spectral parameters of heart rate variability and respiration in human volunteers. *J. Interdiscip. Cycle Res.* **21**, 17–24 https://doi.org/10.1080/09291019009360022 (1990).
59. Shapiro, S. S. & Wilk, M. B. An analysis of variance test for normality (complete samples). *Biometrika* **52**, 591–611 https://doi.org/10.2307/2333709 (1965).
60. Spearman, C. The proof and measurement of association between two things. *Am. J. Psychol.* **15**, 72–101 https://doi.org/10.2307/1412159 (1904).

Acknowledgements

The authors wish to express their profound appreciation to the Villa Beretta Rehabilitation Research Innovation Institute(VBRRII) for their dedicated oversight and meticulous monitoring of the study participant. The unwavering commitmentof Clinical Director Franco Molteni and his team to clinical rigor and ethical standards was instrumental in ensuring thereliability and integrity of the data collected.In the end, the authors would gratefully acknowledge the King Abdullah University of Science and Technology (KAUST) for the institutional support provided within the experimental protocol approval and management.

Author contributions

E.S. provided data curation, elaboration and pubblication; prepared figures; L.P. and E.S wrote the main manuscript text and reviewed the manuscript.

Funding

This research received no external funding.

Competing interests

The authors declare no competing interests.

Additional information

Correspondence and requests for materials should be addressed to E.S.

Reprints and permissions information is available at www.nature.com/reprints.

Publisher's note Springer Nature remains neutral with regard to jurisdictional claims in published maps and institutional affiliations.

Open Access This article is licensed under a Creative Commons Attribution-NonCommercial-NoDerivatives 4.0 International License, which permits any non-commercial use, sharing, distribution and reproduction in any medium or format, as long as you give appropriate credit to the original author(s) and the source, provide a link to the Creative Commons licence, and indicate if you modified the licensed material. You do not have permission under this licence to share adapted material derived from this article or parts of it. The images or other third party material in this article are included in the article's Creative Commons licence, unless indicated otherwise in a credit line to the material. If material is not included in the article's Creative Commons licence and your intended use is not permitted by statutory regulation or exceeds the permitted use, you will need to obtain permission directly from the copyright holder. To view a copy of this licence, visit http://creativecommons.org/licenses/by-nc-nd/4.0/.

© The Author(s) 2026

This Article in Press is shared early to give you faster access to new research. It is citable and carries a permanent DOI. The final edited version will replace it automatically.